Available online at www.sciencedirect.com
ScienceDirect
Trans. Nonferrous Met. Soc. China 35(2025) 3697−3713
Transactions of Nonferrous Metals Society of China
www.tnmsc.cn

Enhancing Mg−air battery discharge performance with AZ31 anodes using complexing agents as electrolyte additives

Xue-ning LI, Chen-chen ZHAO, Shu-bo LI, Mei WAN, Xian DU, Ke LIU, Wen-bo DU

College of Materials Science and Engineering, Beijing University of Technology, Beijing 100124, China

Received 29 February 2024; accepted 22 November 2024

Abstract: The addition of complexing agents to the electrolyte has been shown to be an effective method to enhance the discharge performance of magnesium−air batteries. In this work, four complexing agents: citric acid (CIT), salicylic acid (SAL), 2,6-dihydroxybenzoic acid (2,6-DHB), and 5-sulfoisophthalic acid (5-sulfoSAL) were selected as potential candidates. Through electrochemical tests, full-cell discharge experiments, and physicochemical characterization, the impact of these complexing agents on the discharge performance of magnesium−air batteries using AZ31 alloy as the anode material was investigated. The results demonstrated that the four complexing agents increased the discharge voltage of the batteries. Notably, SAL could significantly improve the anodic efficiency and the discharge specific capacity, achieving an anodic efficiency of 60.3% and a specific capacity of 1358.3 mA·h/g at a discharge current density of 10 mA/cm^2.

Key words: Mg−air batteries; electrolyte additives; complexing agent; discharge voltage; anodic efficiency

1 Introduction

The magnesium−air (Mg−air) battery, known for its large capacity, high energy density, stable discharge voltage, cost-effectiveness, and light-weight design, is regarded as a promising energy storage device [1−3]. It consists of a Mg or Mg alloy anode that degrades during discharge, an electrolyte, and an air cathode that utilizes atmospheric oxygen as the reactive substance, converting chemical energy into electrical energy. Despite the favorable negative electrode potential (−2.37 V (vs SHE)) and high specific capacity (3833 mA·h/cm^3) of Mg, several technological challenges such as self-corrosion, chunk effect, and low discharge voltage limit its wider application [4,5]. Addressing these issues typically involves microstructural anode modifications [6−20] and the selection of suitable electrolytes.

The electrolyte, which directly interacts with the magnesium anode, plays a crucial role in determining the structure and composition of the surface film on the anode. This film affects the kinetics of the dissolution and hydrogen evolution reactions, as well as the discharge voltage [21−26]. Among various electrolytes, 3.5 wt.% NaCl is often favored for its affordability and ease of handling. However, in the NaCl system, Mg^{2+} ions produced by the dissolution of the anode readily react with OH^- in the solution to form an insoluble $Mg(OH)_2$ deposit on the anode surface. This deposition lowers the anode discharge voltage, resulting in a practical working voltage and energy density of Mg−air batteries that fall short of theoretical values.

Studies have shown that adding inorganic or organic compounds to NaCl electrolytes can significantly influence the discharge performance of

Corresponding author: Chen-chen ZHAO, Tel: +86-10-67392423, E-mail: zhaochenchen@bjut.edu.cn;
Shu-bo LI, Tel: +86-10-67392423, E-mail: lishubo@bjut.edu.cn
https://doi.org/10.1016/S1003-6326(25)66907-X

Mg−air batteries. ZHAO et al [27] utilized chromate (Li_2CrO_4) as an electrolyte additive, which marginally reduced the dissolution rate of the anodic metal and significantly decreased the hydrogen evolution rate but did not improve the discharge voltage. DEYAB [28] added 2.5 mmol/L decyl glucoside to the electrolyte, achieving an 89.7% utilization efficiency for pure Mg anode at a discharge current density of 2 mA/cm^2. However, the effectiveness of these additives relies on the formation of a protective layer, which improves anodic efficiency to some extent but tends to reduce the discharge voltage. Hence, additives that simultaneously increase anodic efficiency and discharge potential are needed. HÖCHE et al [29−31] discovered that the negative difference effect (NDE) in magnesium largely depends on the redeposition of iron. By adding ferric complexing agents like salicylates (SAL) to the electrolyte, iron impurity redeposition can be prevented, reducing anodic self-corrosion and $Mg(OH)_2$ formation. WANG et al [32] investigated the impact of complexing agents like 5-sulfoisophthalic acid (5-sulfoSAL) on the discharge performance of a Mg−0.04wt.%Ca alloy at current densities of 0.5, 1, 5, and 10 mA/cm^2, demonstrating that adding 5-sulfoSAL increased the discharge voltage of the Mg−Ca alloy by 270 mV at 0.5 mA/cm^2. At a current density of 1 mA/cm^2, lower complexing capacity additives like citric acid (CIT) improved the anode efficiency from 53% to 64.7%. ZHOU et al [16] examined the impact of complexing agents like CIT on the discharge performance of AM50 alloy under half-cell conditions at current densities of 5, 10, and 15 mA/cm^2, noting that adding SAL complexing agent at 10 mA/cm^2 increased the anodic efficiency of AM50 alloy from 60.4% to 72.3% [16]. However, current research lacks studies on the effect of complexing agents on the battery performance of commercially cost-effective Mg alloys under full-cell conditions.

In this study, we employed commercial AZ31 Mg alloy as the anode and 3.5 wt.% NaCl as the electrolyte to assemble a Mg−air battery. Four complexing agents with different complexation constants, including CIT, SAL, 2,6-dihydroxybenzoic acid (2,6-DHB), and 5-sulfoSAL, were selected as complexing agents for the electrolyte. Through comprehensive electrochemical performance characterization, battery performance testing at different current densities, and analysis of post-discharge and quasi-in-situ discharge morphologies, we systematically examined the effects of these complexing agents on the discharge behavior of magnesium anodes and the overall performance of Mg−air batteries.

2 Experimental

2.1 Materials and chemicals

The anode material used was commercial AZ31 magnesium alloy, and its composition was analyzed using an inductively coupled plasma emission spectrometer (ICP Optima 8300), as shown in Table 1. The electrolyte used was a 3.5 wt.% NaCl solution, and the selected complexing agents were CIT, SAL, 2,6-DHB, and 5-sulfoSAL, each at a concentration of 0.1 mol/L. According to previous studies [32], CIT was identified as a weak complexing agent, SAL as moderate, and both 2,6-DHB and 5-sulfoSAL as strong complexing agents. The solution with complexing agents was adjusted to a pH of 7.0±0.3 using NaOH, and the pH was measured with a PHB−3 pen-type pH meter.

Table 1 Elemental composition of as-cast AZ31 alloy (wt.%)

Al	Zn	Mg
3.14	0.98	Bal.

2.2 Electrochemical measurement

The electrochemical measurements were carried out on an Autolab electrochemical workstation (Metrohm Autolab PARSTAT 2273) with a standard three-electrode cell configuration. The working electrode was an AZ31 alloy with an exposed surface area of 1 cm^2. A saturated calomel electrode (SCE) served as the reference electrode and a platinum sheet was used as the counter electrode. Electrochemical performance tests included open-circuit potential (OCP), polarization curves, and electrochemical impedance spectroscopy (EIS). Samples were immersed in the electrolyte for 4000 s until the potential stabilized, at which point the OCP value was recorded. Polarization curves were obtained at a constant scanning rate of 0.5 mV/s. The corrosion potential (φ_{corr}) and corrosion current

density (J_{corr}) were calculated from Tafel extrapolation. The EIS test was conducted with a sinusoidal excitation voltage of ±10 mV over a frequency range from 100 kHz to 0.01 Hz, and the EIS data were analyzed using Nova 2.0 software.

2.3 Microstructure characterization

The surface morphology of the alloy after discharge was examined using a field emission scanning electron microscope (SEM, Zeiss GeminiSEM 300). The elemental analysis of the surface was performed with the energy-dispersive spectrometer (EDS) attached to the SEM.

2.4 Full-cell test

Mg−air battery performance was tested using a LAND battery testing system (CT2001A). The air cathode was a C/MnO_2 air electrode provided by Carbon Yang Technology Co., Ltd., China. The AZ31 magnesium alloy anode was machined into a block (1 cm × 1 cm × 0.3 cm) and sealed with epoxy to expose an effective surface area of 1 cm^2. The anode was polished up to 2000# grit sandpaper. Performance tests were conducted at discharge current densities of 1, 10, 20, and 50 mA/cm^2. After discharge, the electrodes were ultrasonically cleaned in a 200 g/L chromic acid and ethanol solution to remove discharge products. The anodic efficiency η (%) and specific capacity (Q_{SC}) (mA·h/g) of the battery were calculated by Eqs. (1) and (2), respectively [32−34]:

$$\eta=\frac{W_{theo}}{W_i-W_f}\times 100\% \quad (1)$$

$$Q_{SC}=\frac{I\cdot t}{W_i-W_f}\times 1000 \quad (2)$$

where W_i (g) and W_f (g) represent the mass of the AZ31 alloy before the experiment and after the removal of discharge products, respectively; W_{theo} (g) refers to the theoretical mass consumption of AZ31 alloy, which can be calculated from Eq. (3) [35]:

$$W_{theo}=\frac{I\cdot t}{F\cdot\sum\left(\frac{x_i\cdot n_i}{m_i}\right)} \quad (3)$$

where I (A) and t (h) represent the applied discharge current and battery testing time, respectively; F is the Faraday constant (26.8 A·h/mol); x_i, n_i and m_i (g/mol) denote the mass fraction, number of exchanged electrons, and the atomic mass of each alloying element, respectively.

The real-time hydrogen evolution during the first 2 h of battery discharge was recorded every 10 min. The experiment was repeated three times to ensure the reliability of the data.

3 Results and discussion

3.1 Electrochemical properties

The OCP values, referred to as φ_{OCP}, of AZ31 alloys in various electrolytes are shown in Fig. 1(a). A gradual increase in φ_{OCP} is observed during the initial stage of immersion, attributed to chemical dissolution, electrolyte penetration, and electrochemical redox reactions on the anode surface when using Cl^--containing solutions as the electrolyte. These processes lead to the accumulation of corrosion products on the alloy surface, which decreases the active surface area of the anode, resulting in an elevated φ_{OCP} [36−38]. Upon adding

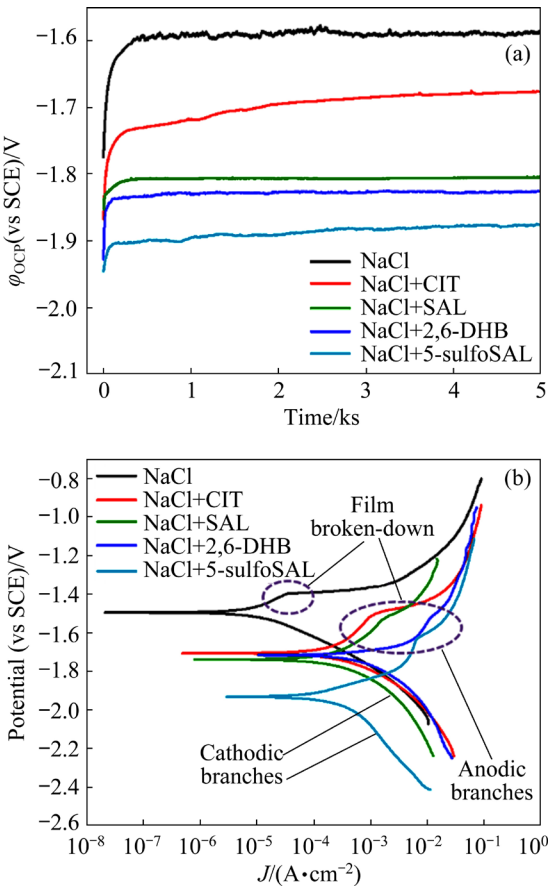

Fig. 1 φ_{OCP} changing with time (a) and polarization curves (b) of AZ31 anodes in different electrolytes

complexing agents, the φ_{OCP} of AZ31 alloy shifts towards more negative values in the order of 5-sulfoSAL < 2,6-DHB < SAL < CIT < NaCl, indicating that the larger the complexation constant with Mg^{2+}, the more negative the φ_{OCP}. As listed in Table 2, the stable φ_{OCP} value of the AZ31 anode in NaCl solution is −1.592 V, while the addition of 5-sulfoSAL results in the most negative φ_{OCP}, stabilizing at −1.862 V, a shift of 270 mV compared to NaCl solution. These results demonstrate that a higher complexation constant with Mg^{2+} leads to a more negative φ_{OCP} value.

Table 2 Electrochemical parameters of AZ31 anode in different electrolytes

Electrolyte	φ_{OCP} (vs SCE)/V	φ_{corr} (vs SCE)/V	J_{corr}/ (μA·cm^{-2})
NaCl	−1.592	−1.4945	6.7755
NaCl+CIT	−1.642	−1.7052	219.57
NaCl+SAL	−1.807	−1.7380	313.79
NaCl+2,6-DHB	−1.827	−1.7157	3825.9
NaCl+5-sulfoSAL	−1.862	−1.9306	5391.4

The polarization behavior of AZ31 alloys in various electrolytes is depicted in Fig. 1(b), showing that the anodic branch corresponds to metal dissolution processes at the anode, while the cathodic branch represents the hydrogen evolution reaction occurring at the cathode [39]. On the anodic branch, the curves become steeper with increasing current density and exhibit inflection points, where the potential is identified as the film rupture potential [40]. During anodic polarization, a passivation film of $Mg(OH)_2$ forms on the alloy surface, and the appearance of inflection points suggests that at these moments, the passivation film is breached. The shape of the curves suggests that after adding complexing agents, the corrosion current density at which film rupture occurs is 2−3 orders of magnitude greater than that in NaCl alone. Furthermore, the corrosion potential is more negative compared to NaCl, implying that the presence of complexing agents enhances anodic activity.

The corrosion potentials (φ_{corr}) and corrosion current densities (J_{corr}) of the AZ31 anode in different electrolytes were calculated using Tafel fitting methods for the cathodic branch [41], as listed in Table 2. The decreasing order of J_{corr} is: 5-sulfoSAL > 2,6-DHB > SAL > CIT > NaCl. This indicates that the addition of complexing agents delays the formation of discharge products, leading to an increase in corrosion current density, which escalates with the increasing complexing ability of the agents.

Electrochemical impedance spectroscopy (EIS) is commonly used to detect minor changes at the electrode/solution interface and to investigate the corrosion processes of materials. The EIS results and equivalent circuit fitting for AZ31 anode in various electrolytes are shown in Fig. 2. In the fitted circuit, respectively, R_s represents the internal resistance of the electrolyte, R_f and CPE_f represent the resistance and capacitance of the oxide film, which are related to the porosity and integrity of the corrosion product layer, respectively, R_{ct} is the charge transfer resistance, and CPE_{dl} represents the double-layer capacitance [31−33]. The fitted values are listed in Table 3. As shown in Fig. 2 and Table 3, the addition of all complexing agents reduced the corrosion resistance of AZ31 anode. The total resistance, R_{total}, defined as the sum of R_f and R_{ct}, is used to characterize the corrosion resistance of the anode in different electrolytes. As shown in Fig. 2(d), the increasing order of R_{total} value in different electrolytes is: 5-sulfoSAL < 2,6-DHB < SAL < CIT < NaCl. This indicates that the addition of complexing agents lowered the impedance of AZ31 alloy in the electrolyte and increased its self-corrosion rate. The stronger the complexing ability, the greater the reduction in impedance, which aligns with the trend observed in the anodic corrosion current density from the polarization curves.

3.2 Battery performance

The discharge curves of Mg−air batteries in different electrolytes at various current densities are presented in Fig. 3. The addition of complexing agents to the electrolyte improves the discharge voltage of the batteries, particularly with 5-sulfoSAL at current densities of 1 and 10 mA/cm^2, where the discharge voltage is the highest. At 1 mA/cm^2, the cell voltage decreases in the following order: 5-sulfoSAL > 2,6-DHB > SAL > CIT > NaCl (Fig. 3(a)). At 20 mA/cm^2, CIT addition results in the highest discharge voltage (Fig. 3(c)). At 1, 10, and 20 mA/cm^2, the Mg−air

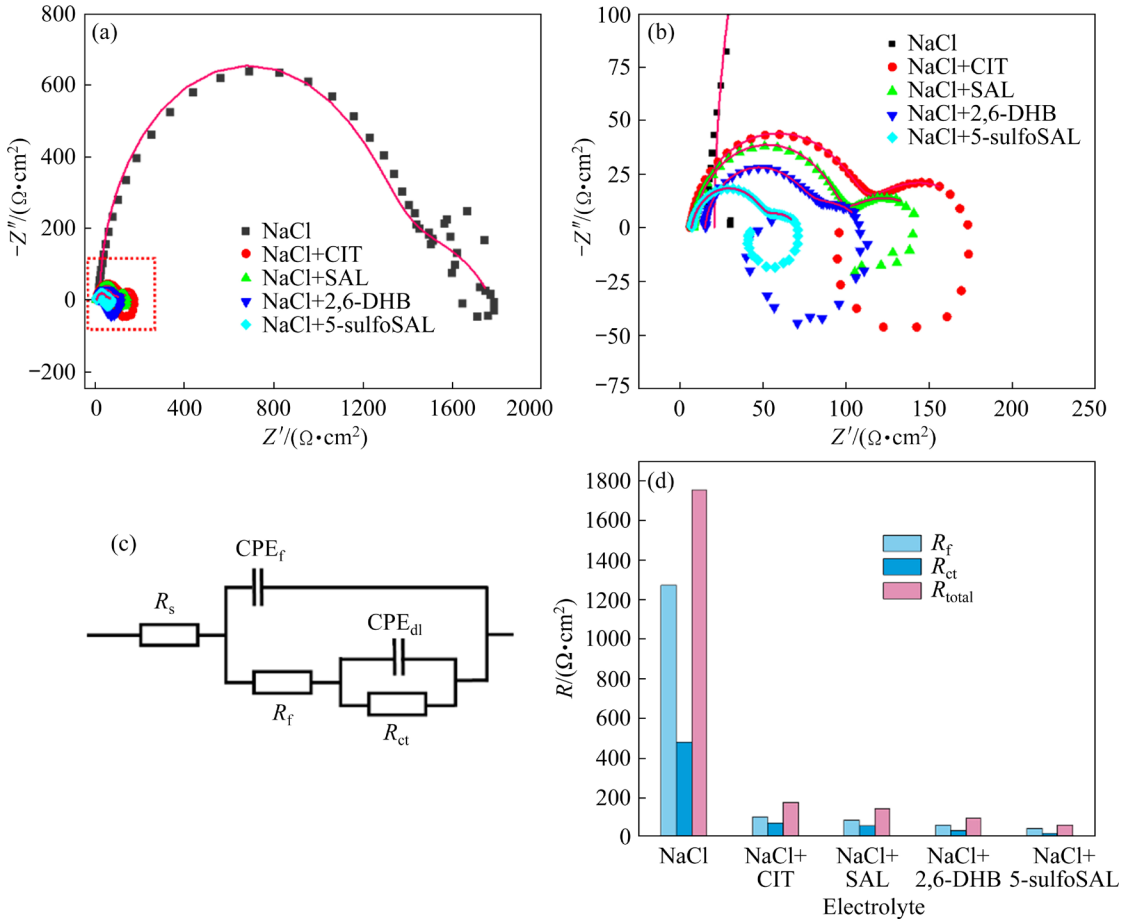

Fig. 2 Electrochemical impedance spectra for AZ31 anodes in different electrolytes: (a) Nyquist plots; (b) Magnification of high-frequency zone of (a); (c) Equivalent circuit; (d) R_f, R_{ct}, and R_{total} values of AZ31 anodes in different electrolytes

Table 3 Electrochemical parameters of AZ31 anodes in different electrolytes obtained by fitting EIS data

Electrolyte	$R_s/(\Omega\cdot cm^2)$	$R_f/(\Omega\cdot cm^2)$	$CPE_f/(\Omega\cdot cm^2\cdot s^n)$		$R_{ct}/(\Omega\cdot cm^2)$	$CPE_{dl}/(\Omega\cdot cm^2\cdot s^n)$	
			Y_0	n		Y_0	n
NaCl	20.965	1271.8	5.9198×10^{-5}	0.99845	481.38	0.000988	0.58954
NaCl+CIT	6.1992	103.580	3.6012×10^{-5}	0.89178	72.773	0.010197	0.63937
NaCl+SAL	8.0589	87.512	3.1731×10^{-5}	0.91612	56.924	0.017967	0.56474
NaCl+2,6-DHB	15.2230	62.129	2.5838×10^{-5}	0.92138	33.362	0.004491	0.63807
NaCl+5-sulfoSAL	7.1411	43.904	3.3161×10^{-5}	0.88286	19.628	0.008808	0.65742

Y_0 is the differential capacitance of the interface; n is the power of the CPE

batteries maintain stable discharge voltages within 2 h, whereas at 50 mA/cm^2, all batteries exhibit significant voltage fluctuations (Fig. 3(d)).

The discharge voltage, anodic efficiency (η), and specific capacity (Q_{SC}) of the AZ31 anode in different electrolytes are shown in Fig. 4 and Table 4. Due to the rapid failure of most batteries within 2 h at 50 mA/cm^2, only the discharge performance at 1, 10 and 20 mA/cm^2 is summarized. As previously mentioned, the addition of complexing agents significantly increases the discharge voltage, with 5-sulfoSAL providing the most notable improvement at 1 and 10 mA/cm^2, increasing the discharge voltage by 10% and 32% compared to the unmodified battery, respectively. At 20 mA/cm^2, CIT achieves the highest discharge voltage of 1.263 V, which is 379 mV higher than that in NaCl solution, marking a 43% increase.

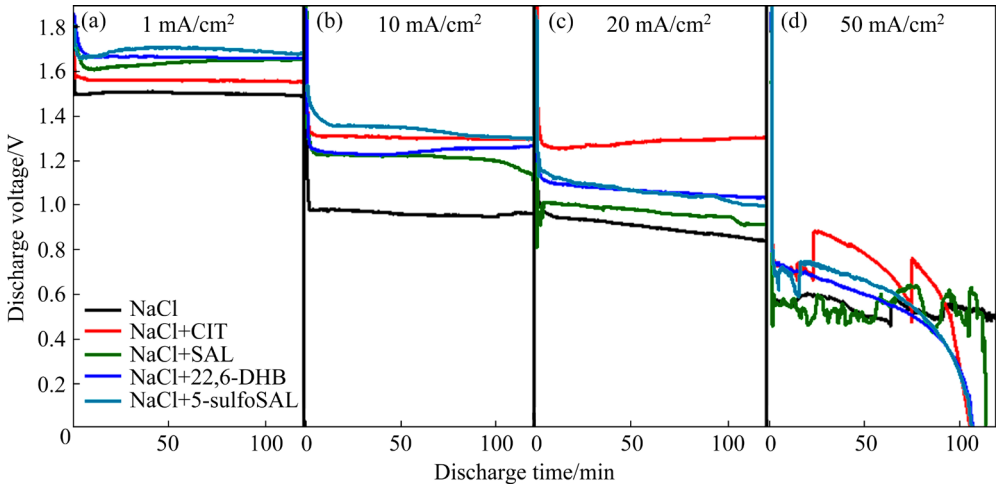

Fig. 3 Discharge curves of AZ31 anodes in different electrolytes for 2 h at various current densities

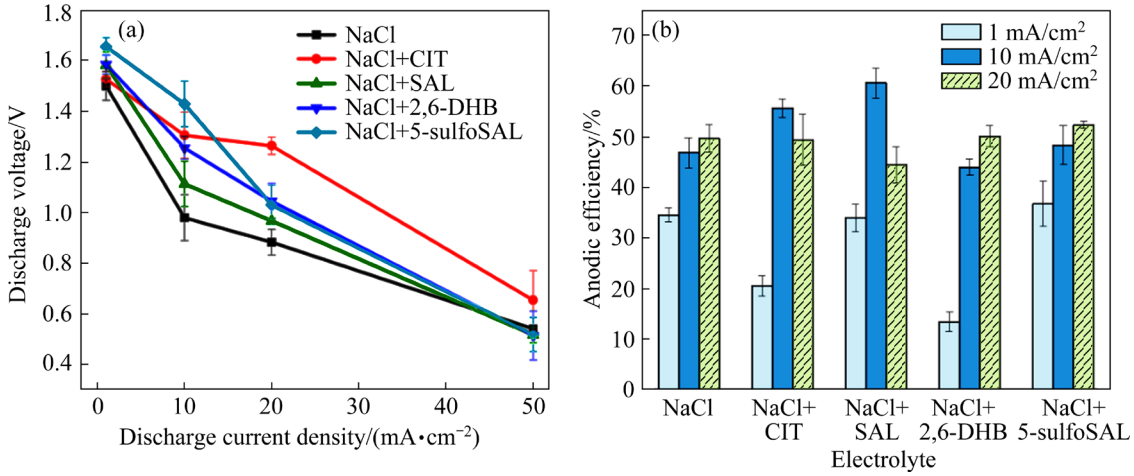

Fig. 4 Discharge voltage (a) and anodic efficiency (b) of AZ31 anodes discharged for 2 h in different electrolytes

Table 4 Discharge properties of AZ31 anodes discharged for 2 h in different electrolytes

Electrolyte	Current density/(mA·cm^{-2})	Discharge voltage/V	Anodic efficiency/%	Specific capacity/(mA·h·g^{-1})
NaCl	1	1.499±0.056	34.6±1.3	770.0±29.6
	10	0.980±0.091	46.8±2.9	1046.1±65.9
	20	0.884±0.050	49.7±2.7	1110.6±61.6
NaCl+CIT	1	1.525±0.031	20.5±1.9	456.7±44.0
	10	1.305±0.091	55.7±1.8	1243.3±41.8
	20	1.263±0.034	49.4±5.1	1103.2±113.4
NaCl+SAL	1	1.581±0.053	34.0±2.7	757.1±60.6
	10	1.113±0.089	60.3±3.0	1358.3±60.1
	20	0.968±0.011	44.3±3.6	993.3±79.9
NaCl+2,6-DHB	1	1.583±0.038	13.4±1.9	299.9±41.7
	10	1.255±0.045	44.0±1.6	970.8±38.3
	20	1.045±0.069	50.1±2.1	1119.6±46.8
NaCl+ 5-sulfoSAL	1	1.654±0.035	36.8±4.4	818.9±98.2
	10	1.428±0.090	48.4±3.8	1080.5±86.5
	20	1.031±0.078	52.4±0.7	1169.7±15.7

Lower discharge current densities result in a slower formation rate of Mg^{2+}. As shown in Fig. 4(b), while the addition of complexing agents increases the discharge voltage at 1 mA/cm^2, it also reduces anodic efficiency and specific capacity due to enhanced magnesium matrix dissolution and severer hydrogen evolution corrosion side reactions at low current densities [31−33]. At 10 mA/cm^2, although SAL does not significantly increase the discharge voltage, it achieves the highest anodic efficiency and specific capacity. Medium-complexation-capacity agents like SAL can delay the formation of discharge product films, promote uniform dissolution of the magnesium matrix, and reduce chunk effects without causing additional loss to the magnesium matrix [16]. With SAL, anodic efficiency η reaches 60.3%, an obvious improvement over that of the NaCl solution (46.8%). However, a sharp drop in η at 20 mA/cm^2 was observed with SAL, likely due to the combined effects of Mg^{2+} complexation, $Mg(OH)_2$ formation, side reactions and product detachment at this current density. The discharge characteristics of Mg−air batteries using various AZ-series alloys as anodes and different aqueous electrolytes are summarized and compared in Table 5. It is evident that the addition of SAL as an electrolyte additive positively impacts discharge performance.

At a low current density of 1 mA/cm^2, the formation rate of Mg^{2+} is slow. The addition of complexing agents allows them to react with Mg^{2+}, thereby increasing the discharge voltage of the battery. Among these agents, 5-sulfoSAL, with the strongest complexing ability, can help to achieve the highest discharge voltage. However, with the Mg^{2+} being complexed, the formation rate and amount of $Mg(OH)_2$ decrease, increasing the active contact area between the anode and the electrolyte, which influences the hydrogen evolution side reaction. Consequently, at 1 mA/cm^2, the addition of complexing agents has little effect on improving the η value. As the discharge current density increases, the generation rate of Mg^{2+} also increases. Due to their unique molecular structures, different complexing agents influence the behavior of water molecules and the structure of the discharge products, which in turn affects anodic efficiency and specific capacity.

3.3 Surface morphology of AZ31 anodes after discharge

SEM images of AZ31 anodes after discharge were obtained and analyzed to further evaluate the deposition of discharge products. The surface morphologies of AZ31 after discharging for 2 h at a current density of 10 mA/cm^2 in different electrolytes are shown in Fig. 5. A layer of discharge products formed on all alloy surfaces, indicating that the addition of complexing agents at 10 mA/cm^2 did not completely prevent the formation of these products. In the NaCl solution, the alloy surface exhibited large, distinct chunks of corrosion products (Fig. 5(a)), with wide and deep cracks surrounding these deposits. The coverage by these products reduced the contact area between the active magnesium matrix and the electrolyte, resulting in the lowest discharge voltage in the NaCl solution. With CIT, the alloy surface also

Table 5 Discharge performance of Mg−air batteries using AZ-series anodes in various aqueous electrolytes

Alloy	Electrolyte	Current density/(mA·cm^{-2})	Discharge voltage/V	Anodic efficiency/%	Specific capacity/(mA·h· g^{-1})	Source
AZ31	3.5 wt.% NaCl+0.1 mol/L SAL	10	1.113	60.3	1358.3	This work
AZ31	0.6 mol/L NaCl+0.02 mol/L Li_2CrO_4	10	0.964	72.2	−	[42]
AZ61	0.6 mol/L NaCl+0.01 mol/L Na_2SiO_3+0.04 mol/L sodium alginate	5	1.234	48.2	1397	[43]
AZ31	0.6 mol/L NaCl+ 0.02 mol/L $Na_3PO_4·12H_2O$	10	1.03	73.1	1068	[44]
AZ91	3.5 wt.% NaCl+0.05 g/L Na_3PO_4	20	1.15	49.1	−	[45]
AZ91	3.5 wt.% NaCl+0.05 g/L SDBS	20	1.141	48.1	−	[45]
AZ91	3.5 wt.% NaCl+0.05 g/L Na_3PO_4+ 0.05 g/L SDBS	20	1.134	48.7	−	[45]

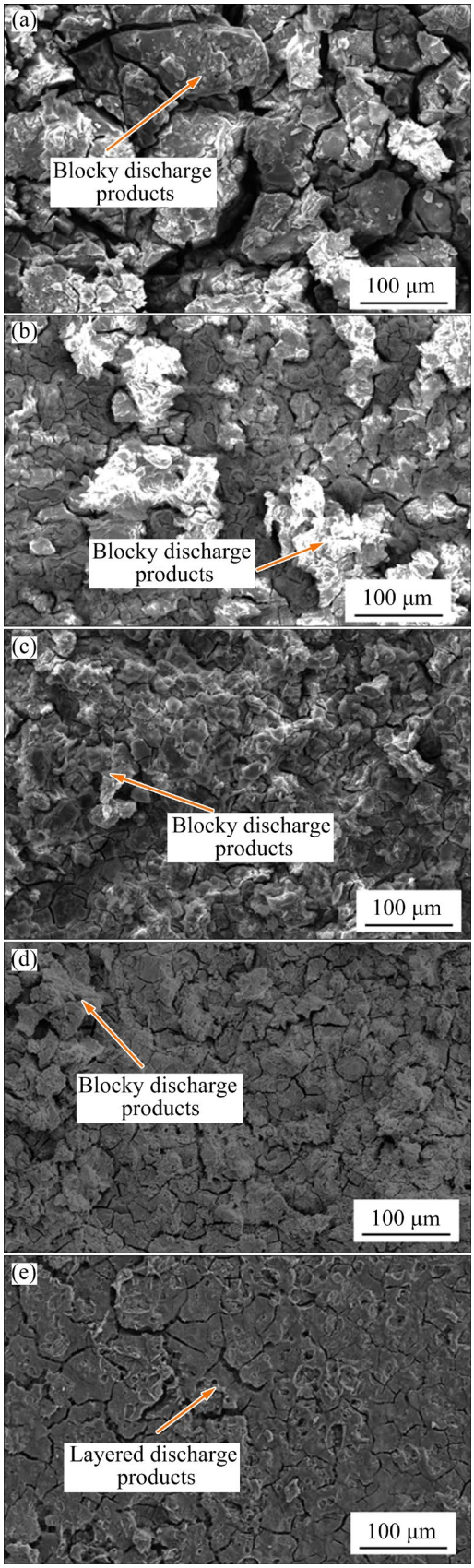

Fig. 5 SEM micrographs of AZ31 anodes obtained after discharging at 10 mA/cm^2 in different electrolytes for 2 h: (a) NaCl; (b) NaCl+CIT; (c) NaCl+SAL; (d) NaCl+2,6-DHB; (e) NaCl+5-sulfoSAL

showed blocky corrosion products surrounded by cracks, but these cracks were narrower and shorter than those in the NaCl solution (Fig. 5(b)). The addition of SAL produced smaller blocky corrosion products with fewer visible cracks, possibly due to the covering effect of the products, making the impact of SAL on discharge voltage at 10 mA/cm^2 less pronounced (Fig. 5(c)). With 2,6-DHB, the alloy surface still exhibited small blocky corrosion products surrounded by fine dendritic cracks (Fig. 5(d)). The addition of 5-sulfoSAL resulted in a layered corrosion product covering the alloy surface, with wide cracks allowing better contact between the electrolyte and magnesium matrix, thereby enhancing the discharge voltage of the battery through the action of the complexing agent (Fig. 5(e)).

The corresponding SEM images of the AZ31 alloy surface after the removal of discharge products are shown in Fig. 6. Except for the electrolyte with 5-sulfoSAL, the alloy surfaces in other solutions exhibited uniform corrosion pits. In the solution with 5-sulfoSAL, the alloy surface showed uneven corrosion with a few deeper corrosion pits. Upon closer inspection, these larger pits contained finer corrosion pits.

According to the results presented in Table 4, the addition of SAL as a complexing agent achieved the highest η and Q_{SC} values for AZ31 anode at a current density of 10 mA/cm^2. To further investigate the reaction process of the anode in electrolytes with and without complexing agents, quasi-in-situ SEM observations of anode surface morphologies were conducted in NaCl and NaCl with adding SAL solutions after 60 and 120 s. As shown in Figs. 7(a1−a5), after 60 s of discharge in NaCl electrolyte, the fine $Mg_{17}Al_{12}$ phase on the AZ31 alloy surface, which served as active sites for the reaction, corroded preferentially, generating $Mg(OH)_2$ in the reaction area. This appeared as raised regions with fine dendritic cracks distributed around them. As discharge progressed to 120 s, the reaction area expanded significantly outward from the initial reaction sites, with an increase in both reaction sites and $Mg(OH)_2$ accumulation. This build-up covered the alloy surface, reducing contact between the magnesium matrix and the electrolyte, thereby decreasing the number of active reaction sites and leading to a lower discharge

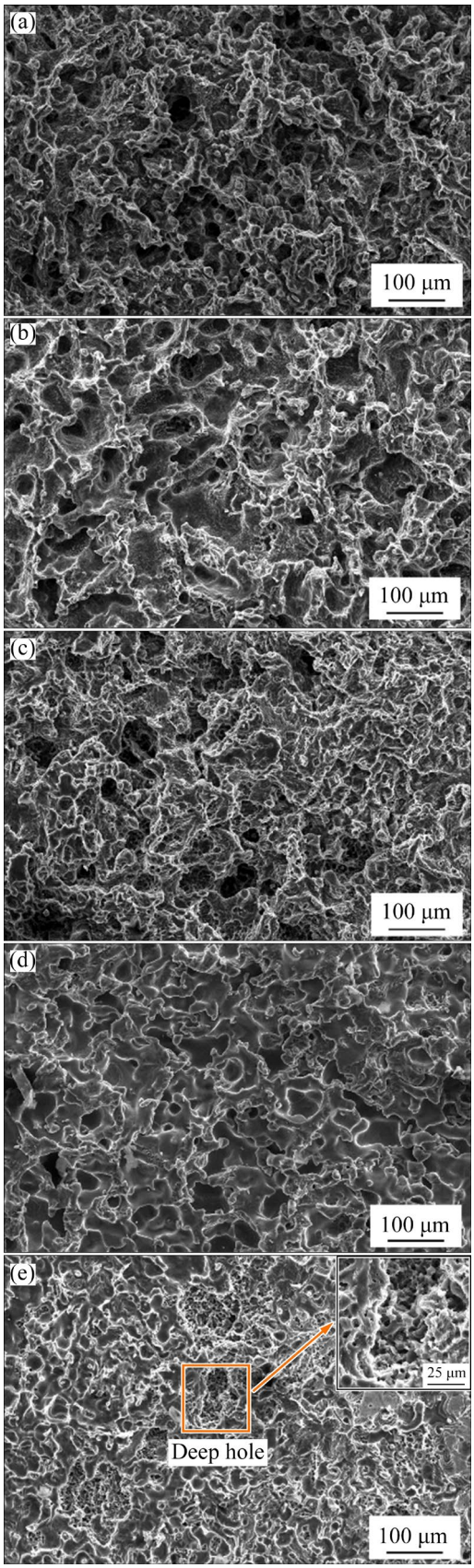

Fig. 6 SEM micrographs of AZ31 anodes discharged in different electrolytes at 10 mA/cm^2 for 2 h after removing surface products: (a) NaCl; (b) NaCl+CIT; (c) NaCl+SAL; (d) NaCl+2,6-DHB; (e) NaCl+5-sulfoSAL

voltage (Figs. 7(b1−b5)). In the NaCl electrolyte with adding SAL complexing agent, after 60 s of discharge, the formation of soluble complexes between SAL and Mg^{2+} delayed the generation of $Mg(OH)_2$, resulting in a concave reaction area. EDS results confirmed the presence of $Mg(OH)_2$, along with network-like cracks within the reaction area (Figs. 7(c1−c5)). Similarly, as the discharge process progressed, by 120 s, the reaction area remained concave, with an increase in reaction sites and a tendency for larger areas to merge (Figs. 7(d1−d5)). $Mg(OH)_2$ still formed within these areas. However, since SAL could not entirely prevent the formation of $Mg(OH)_2$ within the first 120 s, its effect on enhancing the discharge voltage of the battery was limited.

The cross-section morphologies of the anode after discharging for 0.5, 1.5, and 2.0 h at 10 mA/cm^2 in NaCl and NaCl+SAL solutions are shown in Fig. 8. After 0.5 h of discharge, discharge products formed on the alloy surface in both solutions, with a thinner layer observed in the SAL-added solution compared to that in NaCl solution, indicating that the addition of the complexing agent delayed the formation of $Mg(OH)_2$. In the NaCl solution, blocky products were present within the discharge layer, likely due to unreacted magnesium matrix caused by chunk effects. After 1.5 h of discharge, the blocky products remained in the NaCl solution, whereas no such products were observed in the SAL-added solution. The corrosion pits formed in the NaCl solution after 1.5 h reached a depth of 55.61 μm, while that in the SAL-added solution measured about 31.58 μm. After 2.0 h of discharge, the corrosion pits in the NaCl solution deepened to 159.1 μm, compared to 131.8 μm in the SAL-added solution, suggesting that the addition of SAL promoted more uniform corrosion and reduced the occurrence of chunk effects. In summary, the improvement in anode efficiency in SAL-containing electrolytes can be attributed to the mitigation of the chunk effect.

3.4 Real-time hydrogen evolution test results and solution ion changes during discharge

As previously reported, the hydrogen evolution rate of the magnesium anode increases with the positive shift of potential during discharge,

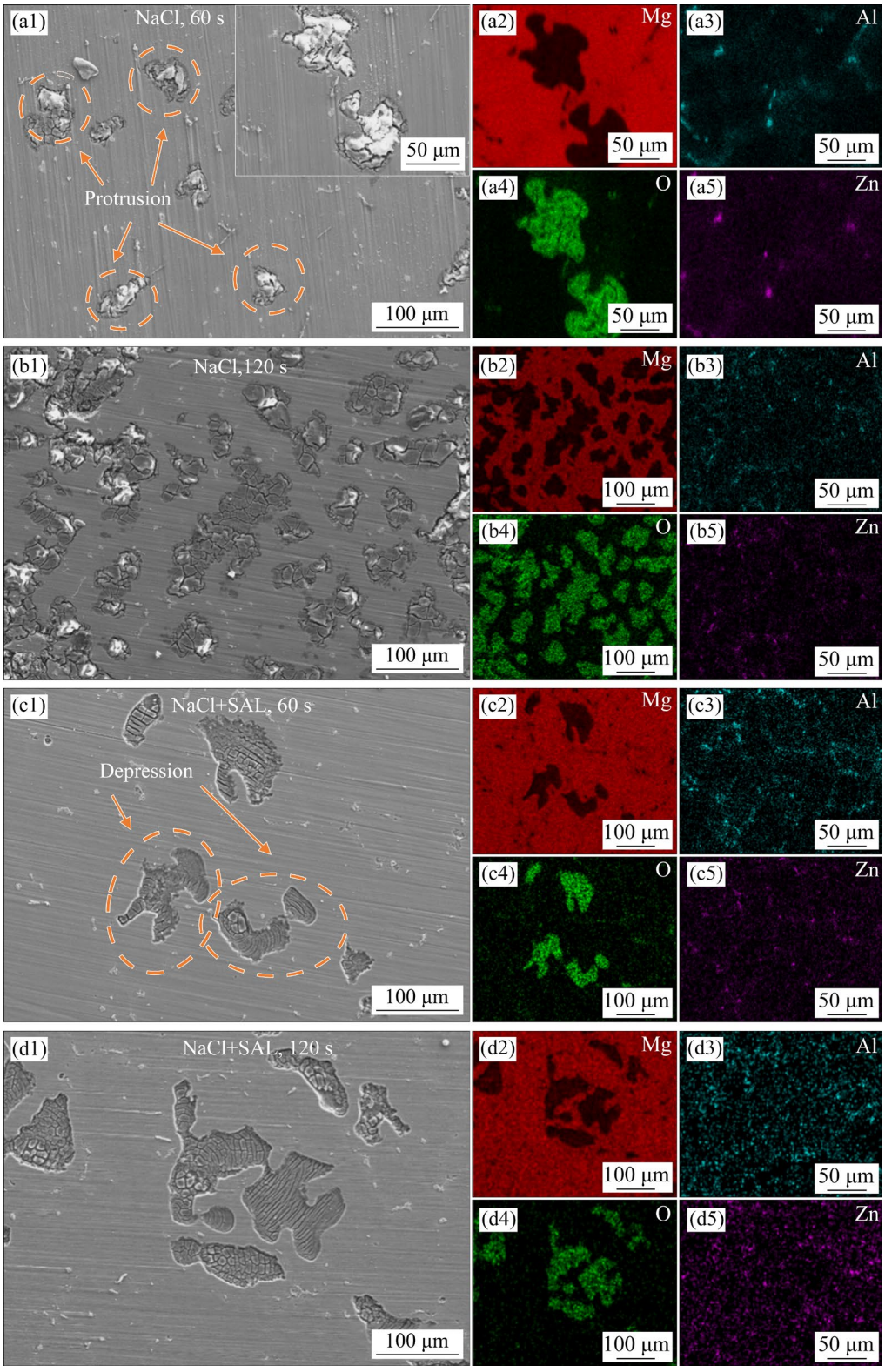

Fig. 7 SEM images and corresponding EDS mapping results of AZ31 anodes after discharging at 10 mA/cm^2

which accelerates the corrosion of the AZ31 anode. This phenomenon, known as NDE, is directly related to the anode efficiency η. As shown in Eq. (4), the total mass loss during discharge consists of three components: theoretical mass loss (W_{theo}), mass loss due to the chunk effect ($W_{\text{chunk effect}}$), and mass loss due to self-discharge ($W_{\text{self-discharge}}$). W_{theo} is determined only by the applied current and discharge time, while $W_{\text{chunk effect}}$ and $W_{\text{self-discharge}}$ have a decisive influence on the actual anodic efficiency.

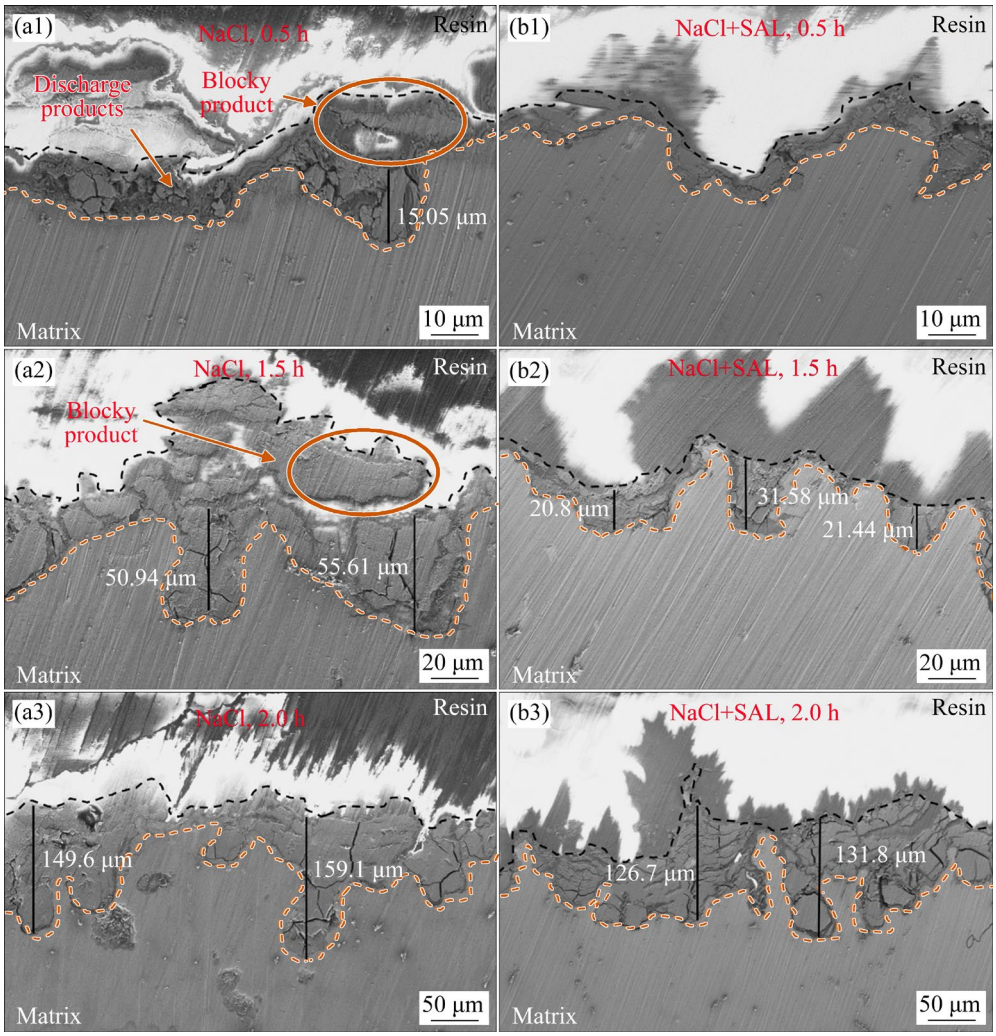

Fig. 8 Cross-section SEM images of AZ31 anodes after discharge at 10 mA/cm^2

$W_{\text{self-discharge}}$ is mainly caused by hydrogen evolution at the anode during discharge [32−35].

$$\Delta W=W_{\text{theo}}+W_{\text{chunk effect}}+W_{\text{self-discharge}} \quad (4)$$

To further analyze the impact of adding complexing agents to the electrolyte, the amount of hydrogen evolved during discharge was recorded, as shown in Fig. 9(a). The amount of hydrogen evolved exhibits a nearly linear relationship with time. Within 2 h of discharge, the addition of 5-sulfoSAL and SAL promoted hydrogen evolution, whereas CIT and 2,6-DHB inhibited the reaction. As indicated by Fig. 9(b), SAL suppressed hydrogen evolution within the first 25 min, but after this period, the amount of hydrogen evolved exceeded that in the NaCl solution. Figure 9(c) quantitatively illustrates the proportion of the alloy mass loss attributed to water reduction and chunk effects. The improvement in η with the addition of CIT and SAL was primarily due to the mitigation of chunk effects, consistent with the previous discussion. The addition of 2,6-DHB inhibited water reduction, thereby reducing mass loss from self-discharge but increasing chunk effects, leading to a decrease in η. This may be related to the structure of the discharge product film [32−35]. The addition of 5-sulfoSAL promoted water reduction without significantly reducing chunk effects, resulting in a lower η value.

Complexing agents can react with metal ions to form soluble complexes, which can be verified by measuring the ion concentrations in the electrolyte after discharge. The concentrations of Mg^{2+}, Al^{3+} and Zn^{2+} in NaCl electrolyte, as well as in electrolytes with adding SAL or 5-sulfoSAL, were determined using ICP after discharging at 10 mA/cm^2 for 2 h. As shown in Fig. 10, the Mg^{2+} concentration in electrolyte increased from

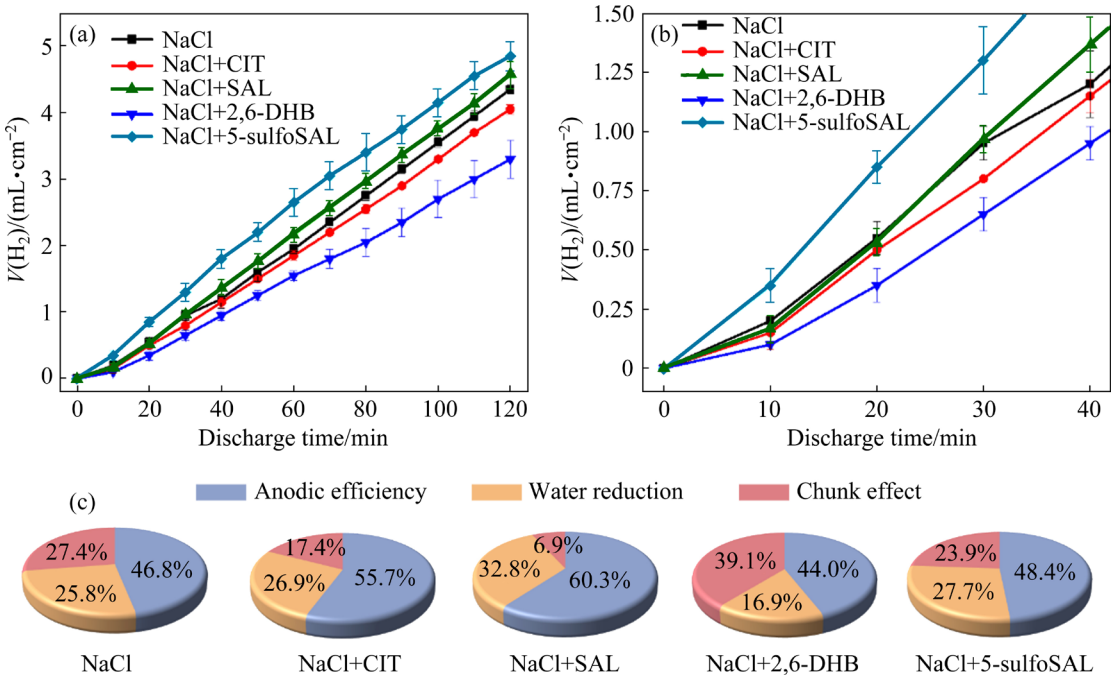

Fig. 9 (a) Real-time hydrogen evolution curves of AZ31 anodes during discharge at 10 mA/cm^2 in different electrolytes; (b) Hydrogen evolution curves for the first 40 min of discharge; (c) Proportion of chunk effect and hydrogen evolution at AZ31 anodes in different electrolytes

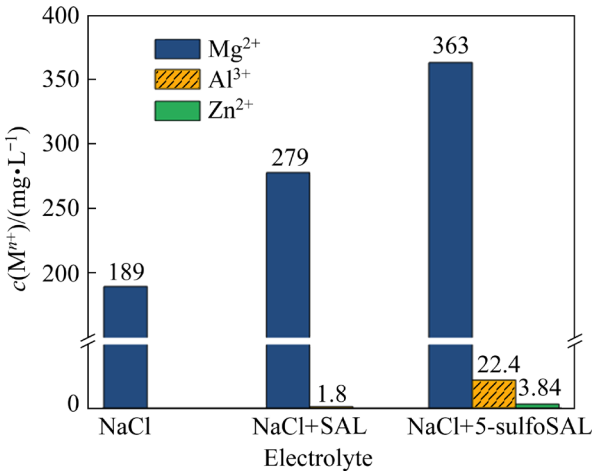

Fig. 10 Concentrations of Mg^{2+}, Al^{3+} and Zn^{2+} in different electrolytes after discharge

189 mg/L in NaCl to 279 mg/L with the addition of SAL and to 363 mg/L with the addition of 5-sulfoSAL. This increase is related to the complexing capability of the agent with Mg^{2+}. 5-sulfoSAL, being a stronger complexing agent, rapidly reacts with Mg^{2+} produced during discharge. As a result, the post-discharge Mg^{2+} concentration with 5-sulfoSAL is nearly double that of the NaCl solution. Since Mg^{2+} is complexed into the electrolyte, the formation of $Mg(OH)_2$ is reduced, increasing the reactive surface area of the magnesium matrix and thereby enhancing the discharge voltage of the battery. However, this increased exposure of the magnesium matrix also accelerates hydrogen evolution. In the NaCl solution, the Al^{3+} concentration was too low to be detected, but with the addition of 0.1 mol/L SAL, the Al^{3+} concentration reached 1.8 mg/L. With 0.1 mol/L 5-sulfoSAL, it increased further to 22.4 mg/L, indicating that complexing agents also react with Al^{3+}, which is related to their complexing ability. No Zn^{2+} was detected in NaCl or SAL-added solutions, but with 5-sulfoSAL, the Zn^{2+} concentration was detected to be 3.84 mg/L, similarly indicating reactions between the complexing agent and Zn^{2+}.

3.5 Discharge mechanism

From the above analysis and discussion, it can be concluded that the SAL interacts with Mg^{2+} and delays the formation of $Mg(OH)_2$ on the surface. However, SAL does not completely prevent the formation of $Mg(OH)_2$, thus offering only limited enhancement to the discharge voltage. The increase in the active magnesium matrix area due to SAL addition promotes hydrogen evolution, leading to

greater water reduction compared to the NaCl solution. Cross-sectional SEM analysis indicates that the improvement in η by SAL is closely related to the mitigation of chunk effects. Through a combination of electrochemical experiments, discharge analysis, surface analysis, and solution ion concentration measurements, the discharge mechanism of AZ31 anode in NaCl electrolyte, with and without SAL, was explored, as depicted in Fig. 11. During the initial stage of discharge, the $Mg_{17}Al_{12}$ phase in the AZ31 alloy acts as active reaction sites and reacts preferentially. In NaCl solution, Mg^{2+} reacts with OH^- to form $Mg(OH)_2$ in the reaction area, leading to a protruding morphology (Fig. 11(a2)). With the addition of SAL, the complexing agent interacts with Mg^{2+}, retarding the formation of $Mg(OH)_2$ and resulting in concave morphology. The reduced $Mg(OH)_2$ coverage increases the active surface area of the anode, thereby enhancing hydrogen evolution and increasing the total amount of hydrogen evolved (Fig. 11(b2)). As the discharge progresses, $Mg(OH)_2$

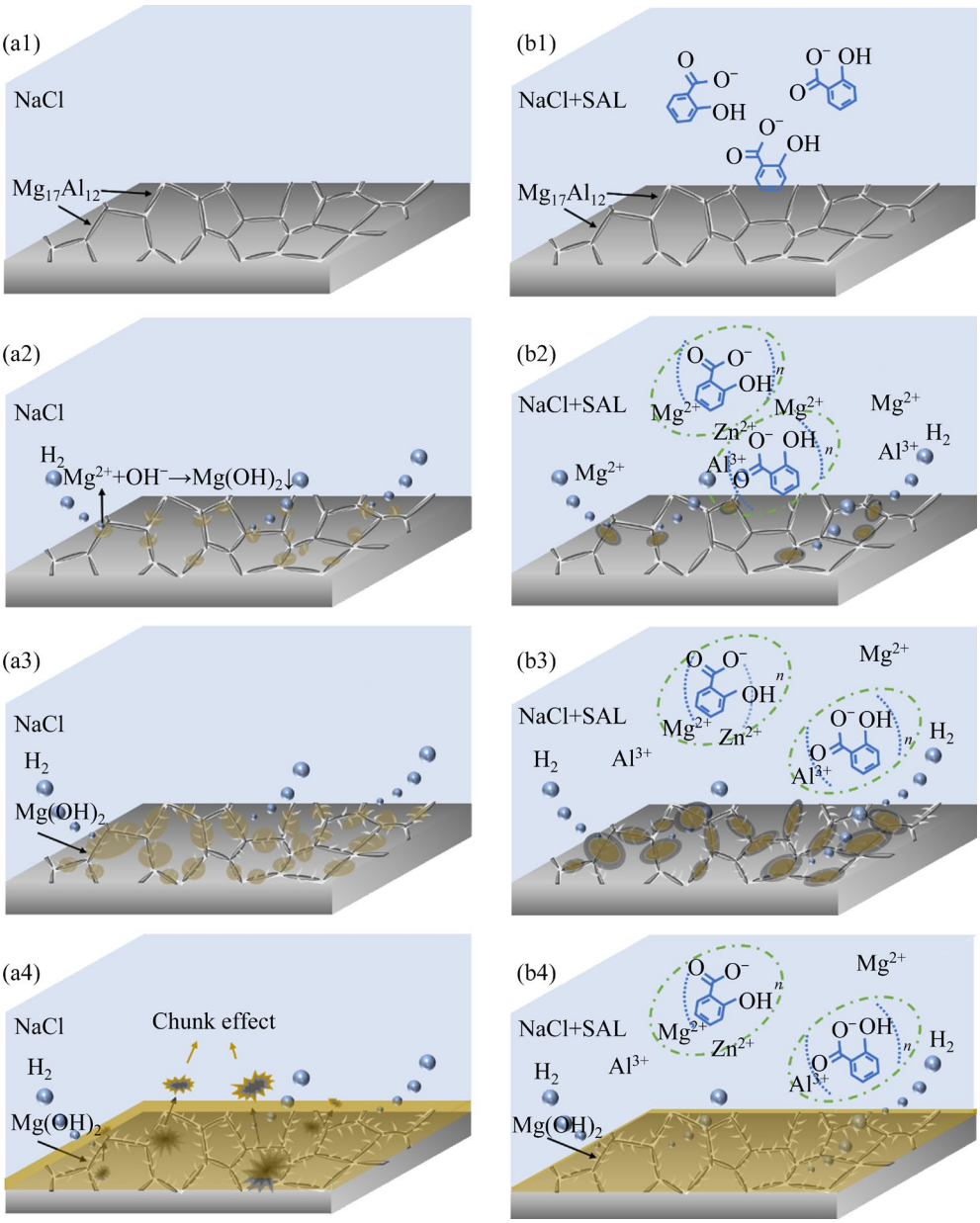

Fig. 11 Schematic illustration of discharge mechanism for AZ31 anodes in NaCl (a1−a4) and NaCl+SAL (b1−b4) electrolytes: (a1, b1) Alloy immersed in different electrolytes; (a2, b2) Secondary phase reacting preferentially, with SAL forming soluble complexes with metal ions, thereby promoting hydrogen evolution from alloy; (a3, b3) Discharge reaction spread across alloy surface; (a4, b4) In NaCl, anode undergoing uneven dissolution, whereas SAL promoting uniform dissolution of alloy, resulting in thinner product layer compared to that in NaCl solution

gradually covers the alloy surface in the NaCl solution (Fig. 11(a3)). In the SAL-added electrolyte, the complexing agent interacts not only with Mg^{2+} but also with Al^{3+} and Zn^{2+} from the AZ31 alloy. However, due to the limited complexing capacity of SAL, it cannot completely prevent $Mg(OH)_2$ formation, leading to a layer of discharge products covering the magnesium matrix surface (Fig. 11(b3)). In the NaCl electrolyte, chunk effects cause portions of the magnesium matrix to detach and fall into the electrolyte without participating in the discharge reaction, reducing anodic efficiency and battery specific capacity (Fig. 11(a4)). The addition of SAL promotes uniform dissolution of the AZ31 alloy, mitigating the occurrence of chunk effects, and thereby effectively enhancing both anodic efficiency and the specific capacity of the battery (Fig. 11(b4)).

3.6 Long-time battery discharge test results

The addition of SAL significantly improved the anodic efficiency and specific capacity of Mg−air batteries at 10 mA/cm^2. Consequently, the discharge life of batteries with NaCl and NaCl+ SAL electrolytes at 10 mA/cm^2 was investigated. As shown in Fig. 12, in the NaCl solution, the anode was depleted after 51 h of discharge, resulting in a voltage drop and battery failure. With the addition of 0.1 mol/L SAL, the voltage drop occurred after 58 h. The addition of SAL extended the battery discharge time by 13.7%. It is evident that SAL, as an electrolyte additive for new energy devices such as Mg−air batteries, can improve the specific capacity and prolong battery discharge life. Additionally, SAL is environmentally friendly, non-toxic, widely available, cost-effective, and easy to obtain, making it promising in the field of metal−air batteries.

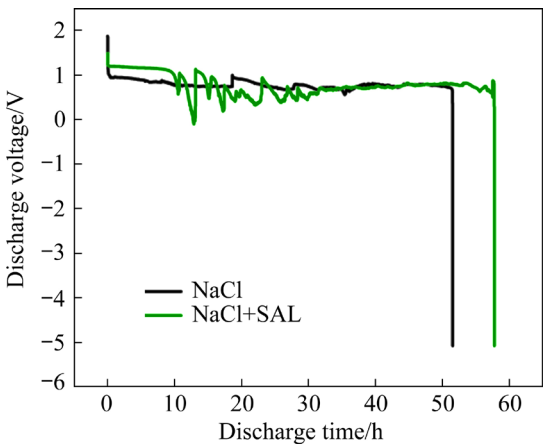

Fig. 12 Discharge curves of AZ31 anode in NaCl and NaCl+ SAL electrolytes at 10 mA/cm^2

4 Conclusions

(1) Complexing agents react with metal ions, delaying the formation of $Mg(OH)_2$, while providing more active regions for discharge, thereby increasing the discharge voltage of the battery.

(2) At a low discharge current density of 1 mA/cm^2, all complexing agents resulted in a decrease in anodic efficiency. At 10 mA/cm^2, different complexing agents had varying effects on hydrogen evolution: 2,6-DHB and CIT inhibited anodic hydrogen evolution, while 5-sulfoSAL and SAL promoted it. SAL, with moderate complexing ability, increased hydrogen evolution during discharge but reduced anodic mass loss due to the chunk effect, thereby enhancing both the anodic efficiency and specific capacity of the Mg−air batteries.

(3) Mg−air batteries with adding SAL exhibited optimal performance at 10 mA/cm^2, achieving the highest anodic efficiency of 60.3% and a specific capacity of 1358.3 mA·h/g. The addition of SAL promoted uniform dissolution of the anode, reducing additional mass and energy loss caused by the chunk effect, thereby effectively improving the discharge performance of the Mg−air battery.

CRediT authorship contribution statement

Xue-ning LI: Methodology, Validation, Formal analysis, Investigation, Visualization, Writing − Original draft; **Chen-chen ZHAO:** Conceptualization, Methodology, Formal analysis, Writing − Original draft, Writing − Review & editing, Visualization, Supervision, Funding acquisition; **Shu-bo LI:** Conceptualization, Formal analysis, Writing − Review & editing, Supervision; **Mei WAN:** Methodology, Validation; **Xian DU:** Writing − Review & editing; **Ke LIU:** Writing − Review & editing; **Wen-bo DU:** Conceptualization, Supervision.

Declaration of competing interest

The authors declare that they have no known competing financial interests or personal relationships that could have appeared to influence the work reported in this paper.

Acknowledgments

This work was supported by the National Natural Science Foundation of China (No. 52001015), the Urban Carbon Neutral Science Innovation Foundation of Beijing University of Technology, China (No. 053000514124601), and the Science and Technology Program of Beijing Municipal Education Commission, China (No. KM201810005007).

References

[1] YANG Yan, XIONG Xiao-ming, CHEN Jing, PENG Xiao-dong, CHEN Dao-lun, PAN Fu-sheng. Research advances in magnesium and magnesium alloys worldwide in 2020 [J]. Journal of Magnesium and Alloys, 2021, 9(3): 705−747.

[2] HAZRI N S, BASRI S, KAMARUDIN S K, ZAINOODIN A M. Critical review on development of magnesium alloy as anode in Mg−air fuel cell and additives in electrolyte [J]. International Journal of Energy Research, 2021, 45(11): 15739−15759.

[3] WANG Ya-ru, SUN Yu-kun, REN Wen, ZHANG Duo, YANG Yang, YANG Jun, WANG Jin-lin, ZENG Xiao-qin, NULI Yan-na. Challenges and prospects of Mg−air batteries: A review [J]. Energy Materials, 2022, 2: 200024.

[4] DENG Min, WANG Lin-qian, HÖCHE D, LAMAKA S V, SNIHIROVA D, VAGHEFINAZARI B, ZHELUDKEVICH M L. Clarifying the decisive factors for utilization efficiency of Mg anodes for primary aqueous batteries [J]. Journal of Power Sources, 2019, 441: 227201.

[5] DENG Min, WANG Lin-qian, VAGHEFINAZARI B, XU Wen, FEILER C, LAMAKA S V, HÖCHE D, ZHELUDKEVICH M L, SNIHIROVA D. High-energy and durable aqueous magnesium batteries: Recent advances and perspectives [J]. Energy Storage Materials, 2021, 43: 238−247.

[6] DING De-yu, DU Yu-hang, TANG Mei-fang, SANG Bo, GUO Ning, ZHANG Hong-ju, GUO Sheng-feng. Corrosion and discharge behavior of Mg−Zn−Mn−Nd alloys as primary Mg−air batteries anode [J]. Transactions of Nonferrous Metals Society of China, 2023, 33(7): 2014−2029.

[7] LI Shu-bo, LI Han, ZHAO Chen-chen, WANG Zhao-hui, LIU Ke, DU Wen-bo. Effects of Ca addition on microstructure, electrochemical behavior and magnesium−air battery performance of Mg−2Zn−*x*Ca alloys [J]. Journal of Electroanalytical Chemistry, 2022, 904: 115944.

[8] ZHENG Tian-xu, HU Yao-bo, ZHANG Yu-xin, YANG Sheng-wei, PAN Fu-sheng. Composition optimization and electrochemical properties of Mg−Al−Sn−Mn alloy anode for Mg−air batteries [J]. Materials & Design, 2018, 137: 245−255.

[9] LIU Xuan, XUE Ji-lai. The role of Al_2Gd cuboids in the discharge performance and electrochemical behaviors of AZ31−Gd anode for Mg−air batteries [J]. Energy, 2019, 189: 116314.

[10] LI Shu-bo, LI Xue-ning, ZHAO Chen-chen, LI Han, LIANG Hong-xing, WANG Shuo, ZHAI Chuan-tian, DU Wen-bo. Boosting the performance of primary Mg−air battery by regulating the second phase in the Mg−2Zn−0.2 Ca anode [J]. Journal of Energy Storage, 2024, 94: 112332.

[11] LI Quan, XIONG Wei, YU Meng-hua, LI Jing, LIU Liu, ZHU Guang, WANG Li-yuan, WANG Jun, YU Si-rong, LIU Er-dong. Effect of Ce content on performance of AZ31 magnesium alloy anode in air battery [J]. Journal of Alloys and Compounds, 2022, 891: 161914.

[12] ZHU Hua-long, LIU Hui, FANG Hong-jie, DAI Yi-long, LI Li, XU Xiang-chun, YAN Yang, YU Kun. Electrochemical performance of Mg−Al−Zn and Mg−Al−Zn−Ce alloys as anodes for Mg−air battery [J]. International Journal of Electrochemical Science, 2018, 13: 11180−11192.

[13] ZOU Qi, LE Qi-chi, CHEN Xing-rui, JIA Yong-hui, BAN Chun-yan, WANG Tong, WANG He-nan, GUO Rui-zhen, REN Liang, ATRENS A. The influence of Ga alloying on Mg−Al−Zn alloys as anode material for Mg−air primary batteries [J]. Electrochimica Acta, 2022, 401: 139372.

[14] ZHANG Yu-wen-xi, HAN Lu, REN Lin-bao, FAN Ling-ling, GUO Yang-yang, ZHOU Ming-yang, QUAN Gao-feng. Effect of yttrium and calcium additions on electrochemical behaviors and discharge performance of AZ80 anodes for Mg−air battery [J]. Transactions of Nonferrous Metals Society of China, 2022, 32(8): 2510−2526.

[15] FENG Yan, LEI Ge, HE Yu-qing, WANG Ri-chu, WANG Xiao-feng. Discharge performance of Mg−Al−Pb−La anode for Mg−air battery [J]. Transactions of Nonferrous Metals Society of China, 2018, 28(11): 2274−2286.

[16] ZHOU Yu-xin, LU Xiao-peng, YANG Lei-yang, TIE Di, ZHANG Tao, WANG Fu-hui. Regulating discharge performance of Mg anode in primary Mg−air battery by complexing agents [J]. Electrochimica Acta, 2021, 370: 137805.

[17] WU Yi-ping, WANG Zhi-feng, LIU Yu, LI Guo-feng, XIE Shao-hui, YU Hui, XIONG Han-qing. AZ61 and AZ61−La alloys as anodes for Mg−air battery [J]. Journal of Materials Engineering and Performance, 2019, 28: 2006−2016.

[18] ZOU Jin-chao, WANG Jun-peng, HUANG Zhi-quan, ZHANG Tao. Effect of multi-pass rolling on the performance of AZ31 magnesium alloy anode in Mg−air battery [J]. Journal of the Brazilian Chemical Society, 2022, 33: 1332−1341.

[19] CHEN Xing-rui, WANG He-nan, ZOU Qi, LE Qi-chi, WEN Cui-e, ATRENS A. The influence of heat treatment on discharge and electrochemical properties of Mg−Gd−Zn magnesium anode with long period stacking ordered structure for Mg−air battery [J]. Electrochimica Acta, 2021, 367: 137518.

[20] CHEN Xing-rui, ZOU Qi, LE Qi-chi, ZHANG Ming-xing, LIU Ming, ATRENS A. Influence of heat treatment on the discharge performance of Mg−Al and Mg−Zn alloys as anodes for the Mg-air battery [J]. Chemical Engineering Journal, 2022, 433: 133797.

[21] NING Ning, FAN Hao-yuan, SONG Shan-shan, ZHANG Jing-lai, WANG Li. Enhancement of the discharge behavior for Mg−air battery by adjusting the chelate ability of ionic liquid electrolyte additives [J]. Journal of Energy Storage, 2023, 72: 108709.

[22] LING Ning, SONG Shan-shan, WANG Cai-li, FAN Hao-yuan, ZHANG Jing-lai, WANG Li. Novel dual-function electrolyte additive for high-power aqueous Mg−air battery: Improvement of both discharge potential and utilization efficiency [J]. Chemical Engineering Science, 2024, 285: 119624.

[23] LIEW S Y, JUAN J C, LAI C W, PAN G T, YANG T C, LEE T K. An eco-friendly water-soluble graphene-incorporated agar gel electrolyte for magnesium-air batteries [J]. Ionics, 2019, 25: 1291−1301.

[24] WANG Yi-fei, PAN Wen-ding, LUO Shi-jing, ZHAO Xiao-long, KWOK H Y H, XU Xin-hai, LEUNG D Y C. High-performance solid-state metal−air batteries with an innovative dual-gel electrolyte [J]. International Journal of Hydrogen Energy, 2022, 47(33): 15024−15034.

[25] MA Jing-ling, HU Peng-fei, JIA Xing-liang, ZHANG Chen-fei, WANG Guang-xin. Organic/inorganic double solutions for magnesium−air batteries [J]. RSC Advances, 2021, 11(13): 7502−7510.

[26] LIU Min, ZHANG Qiang, GAO Jian-xin, LIU Qian-feng, WANG Er-dong, WANG Zhen-bo. $NaBF_4$−dimethyl sulfoxide/NaCl−H_2O biphasic electrolytes for magnesium−air batteries [J]. Ionics, 2022, 28(11): 5243−5250.

[27] ZHAO Yan-Chun, HUANG Guang-sheng, GONG Gui-lin, HAN Ting-zhuang, XIA Da-biao, PAN Fu-sheng. Improving the intermittent discharge performance of Mg−air battery by using oxyanion corrosion inhibitor as electrolyte additive [J]. Acta Metallurgica Sinica (English Letters), 2016, 29: 1019−1024.

[28] DEYAB M A. Decyl glucoside as a corrosion inhibitor for magnesium−air battery [J]. Journal of Power Sources, 2016, 325: 98−103.

[29] LAMAKA S V, VAGHEFINAZARI B, MEI D, PETRAUSKAS R P, HÖCHE D, ZHELUDKEVICH M L. Comprehensive screening of Mg corrosion inhibitors [J]. Corrosion Science, 2017, 128: 224−240.

[30] HÖCHE D, LAMAKA S V, VAGHEFINAZARI B, BRAUN T, PETRAUSKAS R P, FICHTNER M, ZHELUDKEVICH M L. Performance boost for primary magnesium cells using iron complexing agents as electrolyte additives [J]. Scientific Reports, 2018, 8(1): 7578.

[31] VAGHEFINAZARI B, HÖCHE D, LAMAKA S V, SNIHIROVA D, ZHELUDKEVICH M L. Tailoring the Mg−air primary battery performance using strong complexing agents as electrolyte additives [J]. Journal of Power Sources, 2020, 453: 227880.

[32] WANG Lin-qian, SNIHIROVA D, DENG Min, VAGHEFINAZARI B, LAMAKA S V, HÖCHE D, ZHELUDKEVICH M L. Tailoring electrolyte additives for controlled Mg−Ca anode activity in aqueous Mg−air batteries [J]. Journal of Power Sources, 2020, 460: 228106.

[33] WANG Lin-qian, SNIHIROVA D, DENG Min, VAGHEFINAZARI B, HÖCHE D, LAMAKA S V, ZHELUDKEVICH M L. Enhancement of discharge performance for aqueous Mg−air batteries in 2,6-dihydroxy-benzoate-containing electrolyte [J]. Chemical Engineering Journal, 2022, 429: 132369.

[34] DENG Min, HÖCHE D, LAMAKA S V, SNIHIROVA D, ZHELUDKEVICH M L. Mg−Ca binary alloys as anodes for primary Mg−air batteries [J]. Journal of Power Sources, 2018, 396: 109−118.

[35] WANG Nai-guang, LI Wen-ping, HUANG Yi-xiang, WU Gang, HU Ming-chang, LI Guan-zhou, SHI Zhi-cong. Wrought Mg−Al−Pb−RE alloy strips as the anodes for Mg−air batteries [J]. Journal of Power Sources, 2019, 436: 226855.

[36] HEAKAL F E T, FEKRY A M, JIBRIL M B. Electrochemical behaviour of the Mg alloy AZ91D in borate solutions [J]. Corrosion science, 2011, 53(4): 1174−1185.

[37] LI Jia-run, ZHANG Bin-bin, WEI Qin-yi, WANG Ning, HOU Bao-rong. Electrochemical behavior of Mg−Al−Zn−In alloy as anode materials in 3.5 wt.% NaCl solution [J]. Electrochimica Acta, 2017, 238: 156−167.

[38] XIN Yun-chang, LIU Cheng-long, ZHANG Xin-meng, TANG Guo-yi, TIAN Xiu-bo, CHU P K. Corrosion behavior of biomedical AZ91 magnesium alloy in simulated body fluids [J]. Journal of Materials Research, 2007, 22(7): 2004−2011.

[39] LIU Yang, CHENG Wei-li, LIU Yan-hui, NIU Xiao-feng, WANG Hong-xia, WANG Li-fei, CUI Ze-qin. Effect of alloyed Ca on the microstructure and corrosion behavior of extruded Mg−Bi−Al-based alloys [J]. Materials Characterization, 2020, 163: 110292.

[40] WANG Nai-guang, WANG Ri-chu, PENG Chao-qun, FENG Yan. Enhancement of the discharge performance of AP65 magnesium alloy anodes by hot extrusion [J]. Corrosion Science, 2014, 81: 85−95.

[41] CHEN Xing-rui, JIA Yong-hui, LE Qi-chi, WANG He-nan, ZHOU Xiong, YU Fu-xiao, ATRENS A. Discharge properties and electrochemical behaviors of AZ80−La−Gd magnesium anode for Mg−air battery [J]. Journal of Magnesium and Alloys, 2021, 9(6): 2113−2121.

[42] ZHAO Yan-chun, ZHANG Cheng, WANG Jian-kang, ZHANG Hua, ZHANG Peng, XIE Tai-ping, LIU Song-li, PENG Cheng. Influence of Li_2CrO_4 as additive for NaCl electrolyte on Mg−air battery discharge performances [J]. International Journal of Electrochemical Science, 2022, 17(2): 220246.

[43] MA Jing-ling, WANG Guang-xin, LI Ya-qiong, LI Wu-hui, REN Feng-zhang. Influence of sodium silicate/sodium alginate additives on discharge performance of Mg−air battery based on AZ61 alloy [J]. Journal of Materials Engineering and Performance, 2018, 27(5): 2247−2254.

[44] ZHAO Chun-yang, HUANG Guang-sheng, ZHANG Cheng, PENG Cheng, PAN Fu-sheng. Effect of phosphate and vanadate as electrolyte additives on the performance of Mg-air batteries [J]. Materials Chemistry and Physics, 2018, 218: 256−261.

[45] LI Ya-qiong, MA Jing-ling, WANG Guang-xin, REN Feng-zhang, ZHU Yu-jie, SONG Yong-fa. Investigation of sodium phosphate and sodium dodecylbenzenesulfonate as electrolyte additives for AZ91 magnesium−air battery [J]. Journal of the Electrochemical Society, 2018, 165(9): A1713−A1717.

以络合剂为电解液添加剂提升 AZ31 阳极镁−空气电池的放电性能

李雪宁，赵晨辰，李淑波，万 梅，杜 宪，刘 轲，杜文博

北京工业大学 材料科学与工程学院，北京 100124

摘 要：向电解液中加入络合剂是提升镁−空气电池放电性能的有效途径。选用柠檬酸 (CIT)、水杨酸 (SAL)、2, 6-二羟基苯甲酸 (2, 6-DHB)和 5-磺基水杨酸 (5-sulfoSAL) 4 种络合剂，通过电化学实验、全电池放电实验及物理化学性质表征，研究了以上络合剂对以 AZ31 为阳极的镁−空气电池放电性能的影响。结果表明，这 4 种络合剂均提高了电池的放电电压，其中，SAL 可以显著提高阳极效率和电池的放电比容量，当放电电流密度为 10 mA/cm^2 时，阳极效率达到 60.3%，比容量为 1358.3 mA·h/g。

关键词：镁−空气电池；电解液添加剂；络合剂；放电电压；阳极效率

(Edited by Wei-ping CHEN)